Elastic versus inelastic coherent backscattering of laser light by cold atoms: A master-equation treatment

Vyacheslav Shatokhin,[1,2] Cord A. Müller,[3] and Andreas Buchleitner[1]
[1]*Max-Planck-Institut für Physik komplexer Systeme, Nöthnitzer Str. 38, 01187 Dresden, Germany*
[2]*B. I. Stepanov Institute of Physics NASB, 220072 Minsk, Belarus*
[3]*Physikalisches Institut, Universität Bayreuth, 95440 Bayreuth, Germany*
(Received 20 February 2006; published 15 June 2006)

We give a detailed derivation of the master-equation description of the coherent backscattering of laser light by cold atoms. In particular, our formalism accounts for the nonperturbative nonlinear response of the atoms when the injected intensity saturates the atomic transition. Explicit expressions are given for total and elastic backscattering intensities in the different polarization channels, for the simplest nontrivial multiple-scattering scenario of intense laser light multiply scattering from two randomly placed atoms.

DOI: 10.1103/PhysRevA.73.063813 PACS number(s): 42.50.Ct, 42.25.Dd, 32.80.-t, 42.25.Hz

I. INTRODUCTION

Localization phenomena in disordered systems have become a subject of intense research [1,2], since they highlight the fundamental role of interference effects for wave propagation. A prominent example is the coherent backscattering (CBS) of light in dilute, disordered media, a hallmark of weak localization. CBS manifests itself in the enhanced backscattering of the injected radiation, due to the constructive interference between time-reversed pairs of multiple-scattering amplitudes along a given sequence of scatterers, which prevails even after disorder averaging. This remarkable effect was observed for the first time with light scattering from suspensions of polysterene particles [3], but recently has also been reported for laser light scattering from clouds of cold atoms [4–6]. With such quantum scatterers—possessing an internal electronic structure which can be probed by the scattering light field in a controlled way (e.g., by the appropriate choice of the laser frequency and/or of the atomic species)—additional decoherence processes are brought into play, which fundamentally affect the radiation transport across the scattering medium. Elastic Raman processes on degenerate atomic transitions driven by the injected field change its polarization, like spin flips of electrons scattering from lattice impurities [7]. Inelastic processes are induced by intense driving of the atomic transition, leading to its saturation and a nonlinear response of the atom [8], manifest in the emission of photons with frequencies different from the one injected.

Both these decoherence mechanisms reduce the CBS intensity, occur in general simultaneously, and are experimentally very well controlled. Hence, experiments on the multiple scattering of coherent radiation on atomic scatterers provide an ideal testing ground for a detailed analysis of coherent quantum transport in disordered media and of its sensitivity towards various sources of decoherence. Furthermore, if we consider CBS and weak localization as a precursor of strong (i.e., Anderson) localization, decoherence phenomena affecting CBS are likely to become detrimental for the latter. Anderson localization of light, however, is an important experimental target, for fundamental as well as for technological reasons. Consequently, beyond its fundamental interest, a detailed theoretical and experimental understanding of disorder- and/or decoherence-induced transport phenomena is highly desirable for possible applications, which currently emerge, e.g., in the area of random lasers [9].

While the impact of elastic spin-flip processes on the CBS signal is nowadays well understood, with quantitative accordance between experiment and theory [10], nonlinear processes due to the saturation of atomic transitions still challenge our theoretical understanding. On the one hand, perturbative approaches are, by definition, badly suited for the regime of strongly driving intensities. On the other hand, exact solutions which take into account arbitrarily high multiple-scattering orders are prohibitive, due to the exponentially increasing number of contributing scattering paths and of coupled internal states of the atomic scatterers. Different approaches are presently pursued in the attempt to achieve a better understanding of CBS in this parameter regime. These range from diagrammatic techniques [11], over Langevin equations [12], to a master-equation treatment [13], for a small number of atoms. In the present paper, we give a detailed account of the latter approach.

We will focus on the scenario set by the first experimental study of saturation-induced effects on the CBS signal, performed with cold Sr atoms [6]. In these experiments, the injected laser was near resonant with the $^1S_0 \rightarrow {}^1P_1$ transition, which has a nondegenerate ground state and thus leaves no room for spin-flip processes. Consequently, only inelastic scattering could cause decoherence and thus reduce the CBS signal. This was indeed experimentally observed already for moderate values of the atomic saturation parameter

$$s = \Omega^2/2(\delta^2 + \gamma^2). \tag{1}$$

Ω is the driving-induced Rabi frequency, γ half the spontaneous decay rate of the excited atomic level, and $\delta = \omega_L - \omega_0$ the detuning of the injected laser frequency ω_L from the exact atomic transition frequency ω_0; see Fig. 1.

While our formalism to be unfolded hereafter is not restricted to a treatment of atomic transitions with nondegenerate ground states, this specialization allows for a more transparent presentation and, in particular, for a clear identification of the various inelastic processes which intervene.

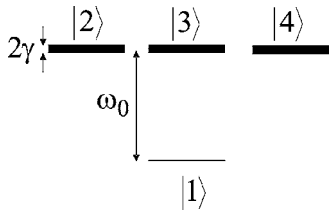

FIG. 1. Level scheme of a $J_g=0\rightarrow J_e=1$ dipole transition, with atomic transition frequency ω_0, and natural linewidth 2γ. The sublevels $|1\rangle$ and $|3\rangle$ have magnetic quantum number $m=0$. Sublevels $|2\rangle$ and $|4\rangle$ correspond to $m=-1$ and $m=1$, respectively.

The paper is organized as follows: The next section starts out with a general Hamiltonian formulation of the dynamics of N atoms under coherent external driving and coupled to the electromagnetic vacuum. A master-equation for the time evolution of the atomic degrees of freedom constitutes the central building block of the theory. Explicit expressions for the (back)scattering intensities in arbitrary polarization channels are derived, in terms of the steady-state quantum-mechanical expectation values of atomic dipoles and of dipole-dipole correlation functions. Expansion of these to second order in the dipole-dipole interaction constant between pairs of atoms finally allows us to present analytic expressions for the polarization-filtered backscattering signal, assuming that double-scattering processes provide the dominant contribution. Accordingly, we restrict our final evaluation to the case of light scattering from two, randomly placed atoms. Section III provides a recipe of how to perform the disorder average, before Sec. IV presents quantitative results for the different polarization channels. Section V concludes the paper.

II. MASTER-EQUATION APPROACH TO COHERENT BACKSCATTERING

A. Full N-atom master-equation

We start with a general formulation of the Hamiltonian describing N identical, motionless atoms with an isotropic dipole transition coupled to the quantized photon reservoir and driven by a quasiresonant (classical) laser field. The total Hamiltonian of the system,

$$H = H_{\mathrm{A}} + H_{\mathrm{F}} + H_{\mathrm{AF}} + H_{\mathrm{AL}}, \tag{2}$$

contains the free atomic Hamiltonian H_{A}, the free field Hamiltonian H_{F}, and the atom-field coupling H_{AF}, as well as the atom-laser coupling H_{AL}:

$$H_{\mathrm{A}} = \hbar\,\omega_0 \sum_{j=\alpha}^{N} \mathbf{D}_\alpha^\dagger \cdot \mathbf{D}_\alpha, \tag{3}$$

$$H_{\mathrm{F}} = \hbar \sum_{\mathbf{k},s} \omega_k a_{\mathbf{k},s}^\dagger a_{\mathbf{k},s}, \tag{4}$$

$$H_{\mathrm{AF}} = \hbar \sum_{\alpha=1}^{N} \sum_{\mathbf{k},s} [\kappa_{\mathbf{k}}^*(\mathbf{r}_\alpha) a_{\mathbf{k},s}^\dagger (\mathbf{D}_\alpha \cdot \boldsymbol{\varepsilon}_{\mathbf{k},s}) + \kappa_{\mathbf{k}}(\mathbf{r}_\alpha) a_{\mathbf{k},s} (\mathbf{D}_\alpha^\dagger \cdot \boldsymbol{\varepsilon}_{\mathbf{k},s}^*)], \tag{5}$$

$$H_{\mathrm{AL}} = -\frac{\hbar}{2} \sum_{\alpha=1}^{N} [\Omega_\alpha e^{-i\omega_L t} (\mathbf{D}_\alpha^\dagger \cdot \boldsymbol{\varepsilon}_L) + \Omega_\alpha^* e^{i\omega_L t} (\mathbf{D}_\alpha \cdot \boldsymbol{\varepsilon}_L^*)]. \tag{6}$$

Here, $\mathbf{D}_\alpha^{(\dagger)}$ is the lowering (raising) operator for the isotropic dipole transition (see Fig. 1) at the resonance frequency ω_0 of atom α, defined by

$$\mathbf{D}_\alpha = -\hat{\mathbf{e}}_{-1}\sigma_{12}^\alpha + \hat{\mathbf{e}}_0 \sigma_{13}^\alpha - \hat{\mathbf{e}}_{+1}\sigma_{14}^\alpha. \tag{7}$$

The $\sigma_{kl}^\alpha \equiv |k\rangle_\alpha \langle l|_\alpha$ mediate transitions between the electronic states of atom α and

$$\hat{\mathbf{e}}_{\pm 1} = \mp \frac{1}{\sqrt{2}} (\hat{\mathbf{e}}_x \pm i\hat{\mathbf{e}}_y), \quad \hat{\mathbf{e}}_0 = \hat{\mathbf{e}}_z \tag{8}$$

are the unit vectors of the spherical basis. In the free-field Hamiltonian, $a_{\mathbf{k},s}^{(\dagger)}$ annihilates (creates) a photon in the reservoir mode with wave vector $\mathbf{k}$ and transverse polarization $\boldsymbol{\varepsilon}_{\mathbf{k},s}$, where s is the polarization index.

The interaction Hamiltonians H_{AF} and H_{AL} are written in rotating wave and dipole approximation. The coupling constant between atom α, located at point $\mathbf{r}_\alpha$, and the vacuum mode $(\mathbf{k},s)$ reads

$$\kappa_{\mathbf{k}}(\mathbf{r}_\alpha) = -id\left(\frac{\omega_k}{2\hbar\,\epsilon_0 V}\right)^{1/2} e^{i\mathbf{k}\cdot\mathbf{r}_\alpha}, \tag{9}$$

where d is a reduced matrix element, ϵ_0 is the permittivity of the vacuum, and V is the quantization volume. The coupling of atom α to the laser field

$$\mathbf{E}_L(\mathbf{r}) = \boldsymbol{\varepsilon}_L \mathcal{E} e^{i(\mathbf{k}_L\cdot\mathbf{r}-\omega_L t)} + \mathrm{c.c.} \tag{10}$$

is characterized by a position-dependent Rabi frequency

$$\Omega_\alpha = \frac{2d\mathcal{E}}{\hbar} e^{i\mathbf{k}_L\cdot\mathbf{r}_\alpha} \equiv \Omega e^{i\mathbf{k}_L\cdot\mathbf{r}_\alpha}. \tag{11}$$

The figure of merit in our present study is the average value of the stationary intensity $I(\mathbf{r})$ with polarization $\boldsymbol{\varepsilon}$, scattered in a direction close to backscattering $-\mathbf{k}_L$:

$$I(\mathbf{r}) = \lim_{t\rightarrow\infty} \langle [\boldsymbol{\varepsilon}\cdot\mathbf{E}^{(-)}(\mathbf{r},t)][\boldsymbol{\varepsilon}^*\cdot\mathbf{E}^{(+)}(\mathbf{r},t)]\rangle. \tag{12}$$

$\mathbf{E}^{(-/+)}(\mathbf{r},t)$ is the negative/positive frequency component of the source field operators, given by the superposition of the retarded fields radiated by all atomic dipoles, which is projected onto the polarization vector $\boldsymbol{\varepsilon}$, upon detection,

$$\boldsymbol{\varepsilon}^*\cdot\mathbf{E}^{(+)}(\mathbf{r},t) = \frac{\omega_0^2}{4\pi\varepsilon_0 c^2 r} \sum_{\alpha=1}^{N} \boldsymbol{\varepsilon}^*\cdot\mathbf{D}_\alpha(t_\alpha) e^{-i\mathbf{k}\cdot\mathbf{r}_\alpha}, \tag{13}$$

with $t_\alpha = t - |\mathbf{r}-\mathbf{r}_\alpha|/c$ and $\mathbf{k}$ the wave vector with the wavelength of the injected laser radiation, pointing in the observation direction (note that all the nontrivial spectral information is contained in the time dependence of the atomic dipole correlation function). This expression follows immediately from generalizing familiar expressions for the far field radiated by a single atom [14] to the present case of an atomic cloud, with the cloud's diameter much smaller than the distance to the detector.

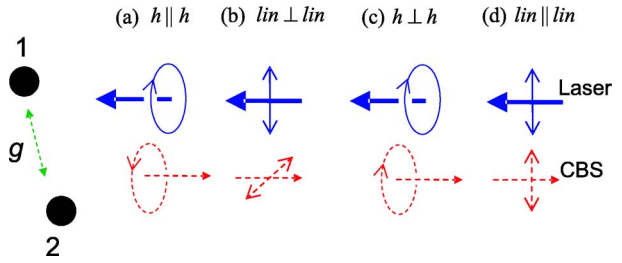

FIG. 2. (Color online) Elementary configuration for the polarization-selective detection of the coherent backscattering signal (CBS) (dashed arrows) from laser light (thick arrows) scattering on two atoms 1 and 2 (black circles). The dipole-dipole coupling strength between the atoms is given by the coupling constant g. Backscattered photons are detected in four polarization channels: (a) right circular in, left circular out (with respect to a fixed observation direction; $h \| h$); (b) linear in, orthogonal linear out ($\text{lin} \perp \text{lin}$); (c) right circular in, right circular out ($h \perp h$); (d) linear in, parallel linear out ($\text{lin} \| \text{lin}$). Note that in cases (c) and (d) CBS appears on the background of single scattering from independent atoms.

The total scattered intensity is then obtained by inserting Eq. (13) and its conjugate into Eq. (12), and reads, up to a prefactor,

$$I = \sum_{\alpha,\beta=1}^{N} \langle [\boldsymbol{\varepsilon} \cdot \mathbf{D}_{\alpha}^{\dagger}][\boldsymbol{\varepsilon}^{*} \cdot \mathbf{D}_{\beta}] \rangle_{\text{ss}} e^{i\mathbf{k}\cdot\mathbf{r}_{\alpha\beta}}, \tag{14}$$

where "ss" stands for *steady state* and $\mathbf{r}_{\alpha\beta} \equiv \mathbf{r}_{\alpha} - \mathbf{r}_{\beta}$.

B. Coherent backscattering and polarization channels

The structure of Eq. (14), together with Eq. (7), shows that all three transitions between each atom's electronic levels (see Fig. 1) will in general contribute to the scattered light intensity—the relative weights of their contributions depend on the observation direction and on the detected polarization channel.

The unit polarization vector $\boldsymbol{\varepsilon}$ may be chosen either in a circular or in a linear basis. For circular polarization, it is convenient to use the so-called helicity basis, in which the quantization axis is directed along the probe direction $\mathbf{k}_L$. In the case of linear polarization, the quantization axis is conveniently chosen along the incident polarization vector $\hat{\mathbf{e}}_0$ (perpendicular to $\mathbf{k}_L$). For both choices, $\boldsymbol{\varepsilon}$ has, in general, three nonzero projections on the unit vectors of the spherical basis, at finite angles between $\mathbf{k}$ and $-\mathbf{k}_L$.

From now on, we will use an approximation which is legitimate at small scattering angles ($\mathbf{k}$ is very close to $-\mathbf{k}_L$), a common situation in CBS experiments. One is interested in signals at very small angles $\theta \simeq 1/k\ell$ around the backscattering direction (the mean free path ℓ is the average distance between consecutive scatterers, and $k\ell \gg 1$ in dilute atomic gases). Since the geometric change of $\boldsymbol{\varepsilon}$ varies only with the cosine of the scattering angle $\theta \ll 1$, we can take $\boldsymbol{\varepsilon}$ constant, equal to its value at exact backscattering.

With these conventions, Eq. (14) can be specialized for the four polarization channels traditionally selected in CBS experiments (see Fig. 2).

1. Helicity-preserving channel ($h \| h$)

In the helicity-preserving channel, the incident radiation is circularly polarized and drives either the $|1\rangle \rightarrow |2\rangle$ or the $|1\rangle \rightarrow |4\rangle$ transition. The backscattered light is then observed in the orthogonal polarization channel (with the same helicity, since the propagation direction is reversed) and must be radiated by the $|1\rangle \rightarrow |4\rangle$ or the $|1\rangle \rightarrow |2\rangle$ transition, respectively. Both combinations are completely equivalent, and for the case $\boldsymbol{\varepsilon}_L = \hat{\mathbf{e}}_{+1}$, $\boldsymbol{\varepsilon} = \hat{\mathbf{e}}_{-1}$, the total backscattered intensity reads

$$I = \sum_{\alpha} \langle \sigma_{22}^{\alpha} \rangle_{\text{ss}} + \sum_{\alpha \neq \beta} \langle \sigma_{21}^{\alpha} \sigma_{12}^{\beta} \rangle_{\text{ss}} e^{i\mathbf{k}\cdot\mathbf{r}_{\alpha\beta}}. \tag{15}$$

2. $lin \perp lin$ channel

In the $\text{lin} \perp \text{lin}$ channel, $\boldsymbol{\varepsilon}_L = \hat{\mathbf{e}}_0$. We further assume, without loss of generality, that the laser field is propagating along the x axis, such that the detected photons are polarized along the y axis. In the spherical basis, $\boldsymbol{\varepsilon} = \hat{\mathbf{e}}_y = i(\hat{\mathbf{e}}_{-1} + \hat{\mathbf{e}}_{+1})/\sqrt{2}$, leading to the expression

$$\begin{aligned} I = & \sum_{\alpha} (\langle \sigma_{22}^{\alpha} \rangle_{\text{ss}} + \langle \sigma_{44}^{\alpha} \rangle_{\text{ss}} + \langle \sigma_{24}^{\alpha} \rangle_{\text{ss}} + \langle \sigma_{42}^{\alpha} \rangle_{\text{ss}}) \\ & + \sum_{\alpha \neq \beta} e^{i\mathbf{k}\cdot\mathbf{r}_{\alpha\beta}} (\langle \sigma_{41}^{\alpha} \sigma_{14}^{\beta} \rangle_{\text{ss}} + \langle \sigma_{21}^{\alpha} \sigma_{12}^{\beta} \rangle_{\text{ss}} + \langle \sigma_{41}^{\alpha} \sigma_{12}^{\beta} \rangle_{\text{ss}} \\ & + \langle \sigma_{21}^{\alpha} \sigma_{14}^{\beta} \rangle_{\text{ss}}). \end{aligned} \tag{16}$$

3. Flipped helicity channel ($h \perp h$)

With incident polarization $\boldsymbol{\varepsilon}_L = \hat{\mathbf{e}}_{+1}$ as before, the $h \perp h$ channel corresponds to $\boldsymbol{\varepsilon} = \hat{\mathbf{e}}_{+1}$, such that

$$I = \sum_{\alpha} \langle \sigma_{44}^{\alpha} \rangle_{\text{ss}} + \sum_{\alpha \neq \beta} \langle \sigma_{41}^{\alpha} \sigma_{14}^{\beta} \rangle_{\text{ss}} e^{i\mathbf{k}\cdot\mathbf{r}_{\alpha\beta}}. \tag{17}$$

4. $lin \| lin$ channel

Finally, in the $\text{lin} \| \text{lin}$ channel, the incoming and outgoing photons are linearly polarized along the same axis, $\boldsymbol{\varepsilon}_L = \boldsymbol{\varepsilon} = \hat{\mathbf{e}}_0$, and we obtain

$$I = \sum_{\alpha} \langle \sigma_{33}^{\alpha} \rangle_{\text{ss}} + \sum_{\alpha \neq \beta} \langle \sigma_{31}^{\alpha} \sigma_{13}^{\beta} \rangle_{\text{ss}} e^{i\mathbf{k}\cdot\mathbf{r}_{\alpha\beta}}. \tag{18}$$

The above expressions systematically decompose into two parts: Single-atom, steady-state dipole expectation values express the intensities radiated by individual atoms, while correlation functions of distinct atomic dipoles, multiplied by phases which depend on the relative position of the atoms, account for the interference contribution.

We now show how to evaluate these different steady-state expectation values explicitly, before performing the ensemble average over the atomic positions, in Sec. III.

C. Equations of motion for the atomic correlation functions

The dynamics of the atomic dipole operators' expectation values as well as of the dipole-dipole correlators which enter Eqs. (15)–(18) is governed by the master-equation [15]

$$\langle \dot{Q} \rangle = \sum_{\alpha=1}^{N} \langle \mathcal{L}_\alpha Q \rangle + \sum_{\alpha \neq \beta=1}^{N} \langle \mathcal{L}_{\alpha\beta} Q \rangle, \tag{19}$$

where the Liouvillians $\mathcal{L}_\alpha$ and $\mathcal{L}_{\alpha\beta}$ generate the time evolution of an arbitrary atomic operator Q, for independent and interacting atoms, respectively, and $\langle \cdots \rangle = \mathrm{Tr}[\cdots \rho(0)]$, with $\rho(0)$ being the initial density operator of the N-atom-field system, indicates the quantum-mechanical expectation value.

In the corotating frame with respect to the driving field at frequency ω_L and after the standard electric-dipole, rotating-wave, and Born-Markov approximations, $\mathcal{L}_\alpha$ and $\mathcal{L}_{\alpha\beta}$ read [15]

$$\mathcal{L}_\alpha Q = -i\delta[\mathbf{D}_\alpha^\dagger \cdot \mathbf{D}_\alpha, Q] - \frac{i}{2}[\Omega_\alpha(\mathbf{D}_\alpha^\dagger \cdot \boldsymbol{\varepsilon}_L) + \Omega_\alpha^*(\mathbf{D}_\alpha \cdot \boldsymbol{\varepsilon}_L^*), Q] + \gamma(\mathbf{D}_\alpha^\dagger \cdot [Q, \mathbf{D}_\alpha] + [\mathbf{D}_\alpha^\dagger, Q] \cdot \mathbf{D}_\alpha), \tag{20}$$

$$\mathcal{L}_{\alpha\beta} Q = \mathbf{D}_\alpha^\dagger \cdot \overleftrightarrow{\mathbf{T}}(g, \hat{\mathbf{n}}) \cdot [Q, \mathbf{D}_\beta] + [\mathbf{D}_\beta^\dagger, Q] \cdot \overleftrightarrow{\mathbf{T}}^*(g, \hat{n}) \cdot \mathbf{D}_\alpha, \tag{21}$$

where the radiative dipole-dipole interaction due to exchange of photons between the atoms is described by the tensor $\overleftrightarrow{\mathbf{T}}(g, \hat{\mathbf{n}}) = \gamma g \overleftrightarrow{\mathbf{\Delta}}$. This interaction has a certain strength depending on the distance between the atoms, via

$$g = \frac{3i}{2k_0 r_{\alpha\beta}} e^{ik_0 r_{\alpha\beta}}, \tag{22}$$

with $k_0 = \omega_0 / c$, and on the lifetime of the excited atomic levels, through γ.

The coupling constant $|g| \ll 1$ is small in the far field ($k_0 r_{\alpha\beta} \gg 1$), where near-field interaction terms of order $(k_0 r_{\alpha\beta})^{-2}$ and $(k_0 r_{\alpha\beta})^{-3}$ can be neglected (which, at higher atomic densities, could also be retained in our formalism). The projector $\overleftrightarrow{\mathbf{\Delta}} = \overleftrightarrow{\mathbb{1}} - \hat{\mathbf{n}}\hat{\mathbf{n}}$ on the transverse plane defined by the unit vector $\hat{\mathbf{n}}$ along the connecting line between the atoms α and β is explicitly given through

$$\overleftrightarrow{\mathbb{1}} = -\hat{\mathbf{e}}_{-1}\hat{\mathbf{e}}_{+1} + \hat{\mathbf{e}}_0\hat{\mathbf{e}}_0 - \hat{\mathbf{e}}_{+1}\hat{\mathbf{e}}_{-1}, \tag{23a}$$

$$\hat{\mathbf{n}} = \frac{e^{i\phi}\sin\vartheta}{\sqrt{2}}\hat{\mathbf{e}}_{-1} + \cos\vartheta\hat{\mathbf{e}}_0 - \frac{e^{-i\phi}\sin\vartheta}{\sqrt{2}}\hat{\mathbf{e}}_{+1}. \tag{23b}$$

The angles (ϑ, ϕ), which fix the direction of the connecting vector between two atoms (with respect to the backscattering direction), will have to be averaged over further down [16].

It should be kept in mind here that the master-equation treatment implies a trace over the modes of the free field and that the Markov approximation implies some coarse graining on the time axis. Thus, γ and g are the only remnants of the coupling to the electromagnetic vacuum, giving rise to some effective dynamics of the atomic operators, on time scales which are long with respect to the time scales of single absorption and emission events from and into the electromagnetic reservoir. Only by expansion of the solutions of Eqs. (20) and (21) in powers of g will we be able to distinguish multiple-scattering contributions of increasing order, since, formally, all elastic and inelastic processes are lumped together in Eqs. (20) and (21) by Ω, γ, and g. This renders the master-equation treatment somewhat less transparent or at least less intuitive as compared to the scattering theoretical approach [11], but bears the qualitative improvement of yielding results which are valid for arbitrary saturation parameter s.

Note that the Markovian master-equation (19) ignores retardation effects due to a finite photon propagation time between scatters. This approximation is justified when $\max(r_{\alpha\beta}) \propto \ell \ll c/\gamma$ [15]. In typical experiments with sharply defined, resonant optical-dipole transitions [10], both the condition of diluteness, $k\ell \gg 1$, and of "instantaneous" propagation are very well satisfied.

Equation (19) leads to a system of linear, coupled differential equations with constant coefficients for the atomic correlation functions. The algebra of the N-atom operators is spanned by tensor products of individual operators $\sigma_{kl}^\alpha = |k\rangle_\alpha \langle l|_\alpha$, each acting on the N-fold tensor product of the four-dimensional Hilbert space in which the internal states of a single atom are represented. For the free evolution of a single atom ($N=1$), Q_α can be chosen in a complete orthonormal set of 16 basis operators (see also Sec. II D below, for details).

For our treatment of CBS, we need to include at least two-atoms operators in Eq. (19). For $N=2$, the number of equations in Eq. (19) is $255 = 16^2 - 1$ (there is one constant of motion). In matrix notation, the resulting equation of motion reads

$$\langle \dot{\mathbf{Q}} \rangle = (\mathbf{A} + \mathbf{V})\langle \mathbf{Q} \rangle + \mathbf{j}, \tag{24}$$

where the elements of the vector $\langle \mathbf{Q} \rangle$ are given by the expectation values of the complete orthonormal set of two-atom operators. The elements A_{nm}, V_{nm}, and j_n of the matrices $\mathbf{A}$ and $\mathbf{V}$ and of the vector $\mathbf{j}$ are derived from the equation for the element $\langle Q_n \rangle$ in Eq. (24):

$$\langle (\mathcal{L}_\alpha + \mathcal{L}_\beta) Q_n \rangle = \sum_{m=1}^{255} A_{nm} \langle Q_m \rangle + j_n, \tag{25}$$

$$\langle (\mathcal{L}_{\alpha\beta} + \mathcal{L}_{\beta\alpha}) Q_n \rangle = \sum_{m=1}^{255} V_{nm} \langle Q_m \rangle. \tag{26}$$

From the decomposition of Eq. (24) into Eqs. (25) and (26) it is apparent that the matrix $\mathbf{A}$ generates the evolution of uncoupled atoms, whereas $\mathbf{V}$ describes their interaction via the exchange of photons.

D. Green's matrix and matrix A

In order to solve Eq. (24), we first need its representation in a suitable operator basis. Thereafter, we will derive a solution for *independent* atoms (that is, we will ignore the matrix $\mathbf{V}$, which mediates the interatomic correlations) by a Laplace transform. The thus-established relation between the Green's matrix for the noninteracting two-atom system and the matrix $\mathbf{A}$ will then serve as a basis for a systematic, perturbative treatment of the interacting case, at increasing order in the coupling constant g.

Let us first consider the dynamics of a single four-level system. An expectation value of a single-atom operator Q_α obeys the equation of motion

$$\langle \dot{Q}_\alpha \rangle = \langle \mathcal{L}_\alpha Q_\alpha \rangle, \tag{27}$$

where the superoperator $\mathcal{L}_\alpha$ is given by Eq. (20). The master-equation (27) describes resonance fluorescence of the laser-driven $J_g=0 \rightarrow J_e=1$ atomic dipole transition. Q_α belongs to the complete orthonormal set S^α of 16 operators for the four-level system,

$$Q_\alpha \in S^\alpha = \left\{ \frac{\mathbb{1}^\alpha}{2}, \frac{\mu_1^\alpha}{2}, \frac{\mu_2^\alpha}{2}, \frac{\mu_3^\alpha}{2}, \underbrace{\sigma_{kl}^\alpha (k \neq l = 1, \ldots, 4)}_{12 \text{ operators}} \right\}, \tag{28}$$

where

$$\mathbb{1} = \sigma_{11} + \sigma_{22} + \sigma_{33} + \sigma_{44}, \tag{29a}$$

$$\mu_1 = \sigma_{22} - \sigma_{33} + \sigma_{44} - \sigma_{11}, \tag{29b}$$

$$\mu_2 = \sigma_{22} - \sigma_{33} - \sigma_{44} + \sigma_{11}, \tag{29c}$$

$$\mu_3 = \sigma_{22} + \sigma_{33} - \sigma_{44} - \sigma_{11}. \tag{29d}$$

It is easy to check that for the elements of S^α the orthonormality condition $\mathrm{Tr}[Q_n Q_m^T] = \delta_{nm}$ holds. In this representation, Eq. (27) turns into a linear matrix equation for the vector $\langle \mathbf{Q}_\alpha(t) \rangle$, whose 16 elements are the quantum-mechanical expectation values of the elements of S^α. Since the atomic levels' dynamics are uncoupled, except for the laser-driven transition, it can be solved analytically. The dynamics of the driven transition is equivalent to the one of a two-level system.

For two atoms, $Q^{\alpha\beta} \in S^\alpha \otimes S^\beta$, and the vector of the two-atoms correlation functions,

$$\langle \mathbf{Q}^{\alpha\beta}(t) \rangle = [\langle \mathbb{1}^\alpha \otimes \mathbb{1}^\beta \rangle / 4, \ldots, \langle \sigma_{kl}^\alpha \otimes \sigma_{kl}^\beta \rangle]^T, \tag{30}$$

consists of 256 elements. The evolution operator of *uncoupled* atoms reads

$$e^{\mathcal{L}_0 t} = e^{\mathcal{L}_\alpha t} \otimes e^{\mathcal{L}_\beta t}. \tag{31}$$

A Laplace transform $\int_0^\infty dt e^{-zt} e^{\mathcal{L}_0 t}$ of Eq. (31) gives the Green's function (or resolvent) $G_{\alpha\beta}(z) = (z - \mathcal{L}_0)^{-1}$ of the Liouvillian $\mathcal{L}_0 = \mathcal{L}_\alpha + \mathcal{L}_\beta$. In the two-atom basis $S^\alpha \otimes S^\beta$, $G_{\alpha\beta}(z)$ has a matrix representation $\mathbf{G}_{\alpha\beta}(z)$. This matrix has the following block structure:

$$\mathbf{G}_{\alpha\beta}(z) = \begin{pmatrix} z^{-1} & \vdots & \mathbf{0}^T \\ \cdots & \cdots & \cdots \\ z^{-1}\mathbf{j} & \vdots & \mathbf{G}_0(z) \end{pmatrix}, \tag{32}$$

where the vectors $\mathbf{0}$ (zero vector) and $\mathbf{j}$ have 255 elements and $\mathbf{G}_0(z)$ is the truncated (255×255) Green's matrix. As seen from Eq. (32), the first column of matrix $\mathbf{G}_{\alpha\beta}(z)$ has a pole at $z=0$. This pole appears because the first element of the vector $\langle \mathbf{Q}^{\alpha\beta}(t) \rangle$, $\langle \mathbb{1}^\alpha \otimes \mathbb{1}^\beta \rangle \equiv \mathrm{Tr}\rho_0$, is a constant of motion. All other elements of the vector $\langle \mathbf{Q}^{\alpha\beta}(t) \rangle$ are time dependent. The steady-state solution of the truncated vector, $\langle \mathbf{Q}(t) \rangle$, which is obtained from $\langle \mathbf{Q}^{\alpha\beta}(t) \rangle$ after exclusion of its first element, $\mathrm{Tr}\rho_0$, is defined as $\langle \mathbf{Q} \rangle_{\mathrm{ss}} = \lim_{z \to 0} z \langle \tilde{\mathbf{Q}}(z) \rangle$, where $\langle \tilde{\mathbf{Q}}(z) \rangle$ is the Laplacian image of the vector $\langle \mathbf{Q}(t) \rangle$. This limit is evaluated to give

$$\langle \mathbf{Q} \rangle_{\mathrm{ss}} = \mathbf{G}_0 \mathbf{j}, \tag{33}$$

where $\mathbf{G}_0 \equiv \mathbf{G}_0(0)$. Comparison of Eq. (33) with the steady-state solution of Eq. (25), $\langle \mathbf{Q} \rangle_{\mathrm{ss}} = -\mathbf{A}^{-1}\mathbf{j}$, now shows that $\mathbf{G}_0 \equiv -\mathbf{A}^{-1}$.

E. Perturbative restriction to low scattering orders

A theoretical description of coherent backscattering is relatively simple in two opposite regimes: either in the diffusive regime of fully developed multiple scattering in optically thick media, where long paths or high scattering orders yield the celebrated conical line shape of the CBS signal, or, on the contrary, in the regime of scattering by optically thin media (or in the presence of suppression of interference), where only double scattering needs to be considered [17,18]. Indeed, it is in the double-scattering regime where the first experimental observation of a CBS reduction due to the nonlinear saturation of atomic dipole transitions was reported [6]. We limit our present analytical and numerical analysis to this specific case.

In our master-equation framework, all information on multiple-scattering processes is contained in the correlation functions of dipole-dipole interacting atoms. The double-scattering contribution to the scattered light intensity from a given pair of atoms, resulting from the exchange of two photons between the atoms, is obtained by perturbative expansion of the respective correlation functions to second order in the dipole-dipole coupling constant $|g|$. This contribution depends only on the observables related to the two selected atoms, and not on those of the rest of the atoms in the cloud, since corrections to the mean intensity due to the latter would be of higher order in $|g|$ ($|g|^3$, etc.). Therefore, to find the double-scattering contribution, we will solve the master-equation (19) for two fixed atoms $\alpha = 1, 2$. Subsequently, we have to add up all double-scattering contributions resulting from the atoms located at random positions. In other words, we need to perform appropriate disorder averages of the solution for two fixed atoms.

This setup defines the simplest possible model describing CBS. Indeed, double scattering is the lowest-order process which gives rise to distinct scattering amplitudes that can interfere constructively. Despite its simplicity, this model allows for a qualitative assessment of the impact of nonlinear scattering processes on the CBS signal, whereas propagation effects in the bulk of the scattering medium are beyond its reach. It also needs to be considered that nonlinear scattering processes are induced by high laser intensities, at which atoms are rapidly accelerated out of resonance. Within our model, we neglect this acceleration, by focusing exclusively on the coupling of photons to the internal atomic degrees of freedom. Such an approximation is justified, since the mechanical action of light on atoms can be experimentally com-

pensated by shortening the CBS probe duration, as realized, e.g., in [6].

For our perturbative solution of Eq. (24), we take advantage of the small parameter g in (21) [defined in Eq. (22)] and expand in a power series of $\mathbf{V}$. The nth order

$$\langle \mathbf{Q} \rangle_{\mathrm{ss}}^{[n]} = (\mathbf{G}_0 \mathbf{V})^n \mathbf{G}_0 \mathbf{j} \tag{34}$$

of the stationary solution of Eq. (24) gives the two-atom correlation functions resulting from n exchanged photons and generally includes also recurrent scattering (a photon visits the same atom several times). We recall that, in the regime of elastic scattering from dilute samples of resonant scatterers, higher scattering orders can be accounted for by considering more scatterers, while recurrent scattering is irrelevant [19]. In contrast, as one proceeds to the strong-scattering regime, with denser clouds of resonant scatterers, the effect of recurrent scattering manifests by a gradual reduction of the enhancement factor as compared to its maximum value of 2.0 [20]. We will see in Sec. IV C 1 below that Eq. (34) generally including recurrent scattering contributions is fully compatible with neglecting these in the linear regime.

Total intensities for the double-scattering contribution are given by the third term (proportional to $|g|^2$) of the above expansion of the correlation functions which enter Eqs. (15)–(18), with the general structure

$$\langle \mathbf{Q} \rangle_{\mathrm{ss}}^{[2]} = \mathbf{G}_0 \mathbf{V} \mathbf{G}_0 \mathbf{V} \mathbf{G}_0 \mathbf{j}. \tag{35}$$

Note that the matrix $\mathbf{V}$ depends on $\overleftrightarrow{\mathbf{\Delta}}$, though neither on $\boldsymbol{\varepsilon}_L$ nor on $\boldsymbol{\varepsilon}$. Indeed, information about the laser polarization is carried by the Liouvillian (20), which governs the evolution of independent atoms. As for $\boldsymbol{\varepsilon}$, it does not appear in the equations of motion for the atomic correlation functions at all—but it defines which elements of the vector $\langle \mathbf{Q} \rangle_{\mathrm{ss}}^{[2]}$ contribute to the observed signal, as evident from Eq. (14).

F. Elastic component of double scattering

The total backscattered intensity (14) has a spectral distribution that contains an elastic and, beyond the weak-field limit, also an inelastic component. The detected intensity is the correlation function of the source field amplitudes radiated by the atomic dipoles.

Its elastic component stems from the classically radiating dipoles—i.e., from the nonfluctuating factorized averages $\langle \sigma_{i \neq j}^{\alpha} \rangle$ [8]. Hence, the elastic intensity is given by the product of the expectation values of the atomic dipoles,

$$I^{\mathrm{el}} = \sum_{\alpha,\beta=1}^{N} \langle \boldsymbol{\varepsilon} \cdot \mathbf{D}_{\alpha}^{\dagger} \rangle_{\mathrm{ss}} \langle \boldsymbol{\varepsilon}^{*} \cdot \mathbf{D}_{\beta} \rangle_{\mathrm{ss}} e^{i \mathbf{k} \cdot \mathbf{r}_{\alpha\beta}}. \tag{36}$$

In the helicity-preserving channel $h \| h$, this reads

$$I^{\mathrm{el}} = \sum_{\alpha} |\langle \sigma_{21}^{\alpha} \rangle_{\mathrm{ss}}|^2 + \sum_{\alpha \neq \beta} \langle \sigma_{21}^{\alpha} \rangle_{\mathrm{ss}} \langle \sigma_{12}^{\beta} \rangle_{\mathrm{ss}} e^{i \mathbf{k} \cdot \mathbf{r}_{\alpha\beta}}. \tag{37}$$

Analogous expressions for the elastic component can be derived from Eqs. (16)–(18) in the other channels.

The double-scattering contribution I_2^{el} to the elastic intensity, which we are interested in and which is proportional to $|g|^2$, is obtained from the corresponding power series expansion, Eqs. (34) and (35) of the individual factors entering the above expression, in the coupling constant. In this expansion, there emerge symmetric and asymmetric combinations, like $\langle \sigma_{21}^1 \rangle_{\mathrm{ss}}^{[1]} \langle \sigma_{12}^2 \rangle_{\mathrm{ss}}^{[1]}$, and $\langle \sigma_{21}^1 \rangle_{\mathrm{ss}}^{[2]} \langle \sigma_{12}^2 \rangle_{\mathrm{ss}}^{[0]}$, respectively. To ease the physical interpretation of these various terms, remember that, by virtue of Eq. (34), the superscripts [0], [1], and [2] signal the scattering of a photon from one single atom α ([0]), subsequently from atom α, and then from atom β ([1]), and the rescattering of the same photon from atom α, *after* a first encounter with α and subsequent scattering from β ([2]).

In the $h \| h$ and lin $\perp$ lin channel, only symmetric combinations contribute to the elastic component of the CBS intensity, since the lowest-order expectation value of a single atom's coherence in the analyzed transition (like $\langle \sigma_{12}^2 \rangle_{\mathrm{ss}}^{[0]}$ in the helicity-preserving channel) must vanish: at lowest order, the atom is not coupled to the other atom; nor is the transition directly driven by the injected laser. By the same argument, also the single-scattering intensities from noninteracting atoms [arising from the first sum on the right-hand side of Eq. (37)] are projected out, and an interference signal from purely multiple-scattering sequences is measured in these channels (unless the atoms have a degenerate ground state and can undergo transitions between different Zeeman sublevels [21]).

In the $h \perp h$ and lin $\|$ lin channels, both symmetric and asymmetric combinations of products of the dipole averages contribute.

Altogether, at second order in the coupling constant, the elastic backscattering intensity from two fixed atoms is obtained from evaluation of the zeroth-, first-, and second-order stationary solutions $\langle \mathbf{Q} \rangle_{\mathrm{ss}}^{[0]}$, $\langle \mathbf{Q} \rangle_{\mathrm{ss}}^{[1]}$, and $\langle \mathbf{Q} \rangle_{\mathrm{ss}}^{[2]}$ of Eq. (24). The backscattering intensity from a cloud of *randomly* located atoms is finally derived through an appropriate disorder average.

III. DISORDER AVERAGING

Coherent backscattering is such a surprising effect because it survives the ensemble average over random positions of the scatterers, which destroys all other specklelike interferences. The precise procedure of disorder averaging is important as soon as one is interested in the exact shape and angular width of the CBS cone. Here, we rather focus on the impact of the atomic saturation on the maximum CBS intensity, in the exact backscattering direction. Since saturation effects are independent of the precise averaging prescription, we choose a procedure as simple as possible: an (i) isotropic average of the relative orientation $\hat{\mathbf{n}}$ of the atoms over the unit sphere is followed by (ii) an average of the interatomic distance r_{12} over an interval of the order of laser wavelength, around their typical distance ℓ:

$$\langle \cdots \rangle_{\mathrm{conf}} = \frac{k_L}{4\pi} \int_{\ell - 2\pi/k_L}^{\ell + 2\pi/k_L} dr_{12} \int d\Omega_{\hat{\mathbf{n}}} \cdots . \tag{38}$$

After the evaluation of Eq. (38), the final expression for the backscattering intensity has a general structure which decomposes into "ladder" and "crossed" contributions, respec-

tively. The ladder terms collect the intensities scattered by individual atomic dipoles (in a diagrammatic representation, they arise from the summation of copropagating amplitudes [2] along a sequence of scatterers), in an incoherent sum, whereas the crossed terms stem from the interference of amplitudes radiated by distinct dipoles (counterpropagating amplitudes in a diagrammatic picture) and are garnished by the associated phases. Through this phase factor, the interference part depends on the angle θ between the wave vector $\mathbf{k}$ of the final photon and the backscattering direction $-\mathbf{k}_L$. As an example, the ladder and crossed terms in the $h\|h$ channel read, by virtue of Eq. (15),

$$L_2^{\mathrm{tot}} = \langle\langle\sigma_{22}^1\rangle_{\mathrm{ss}}^{[2]} + \langle\sigma_{22}^2\rangle_{\mathrm{ss}}^{[2]}\rangle_{\mathrm{conf}}, \tag{39}$$

$$C_2^{\mathrm{tot}}(\theta) = 2\,\mathrm{Re}\langle\langle\sigma_{21}^1\sigma_{12}^2\rangle_{\mathrm{ss}}^{[2]} e^{i\mathbf{k}\cdot\mathbf{r}_{12}}\rangle_{\mathrm{conf}}, \tag{40}$$

respectively.

The enhancement factor α, which is the figure of merit for the quantification of CBS, is given by

$$\alpha = 1 + \frac{C_2^{\mathrm{tot}}(0)}{L_2^{\mathrm{tot}}}. \tag{41}$$

An analogous expression for the *elastic* CBS component follows from Eq. (37), with ladder and crossed terms L_2^{el} and $C_2^{\mathrm{el}}(\theta)$.

IV. RESULTS

We now proceed to evaluate the general expressions derived above, for the four typical polarization channels analyzed in the laboratory: $h\|h$, $\mathrm{lin}\perp\mathrm{lin}$, $h\perp h$, and $\mathrm{lin}\|\mathrm{lin}$. Analytical results for vanishing detuning δ will be complemented by some numerical results for $\delta\neq 0$.

A. $h\|h$ channel

1. Total intensity, at zero detuning

In Eqs. (15) and (37) we assumed that the $|1\rangle\rightarrow|4\rangle$ transition is laser driven. Photons with preserved helicity originate from the $|2\rangle\rightarrow|1\rangle$ transitions, and $\boldsymbol{\varepsilon}_L=\hat{\mathbf{e}}_{+1}$, $\boldsymbol{\varepsilon}=\hat{\mathbf{e}}_{-1}$. The total double-scattering intensity for two fixed atoms reads, by virtue of Eqs. (15) and (35), at second order in g and vanishing detuning $\delta=0$:

$$2\,\mathrm{Re}\{\langle\sigma_{21}^1\sigma_{12}^2\rangle_{\mathrm{ss}}^{[2]} e^{i\mathbf{k}\cdot\mathbf{r}_{12}}\} = |g|^2|\overleftrightarrow{\boldsymbol{\Delta}}_{+1,+1}|^2\frac{R_1(s)}{(4+s)P(s)} \times\cos\{(\mathbf{k}+\mathbf{k}_L)\cdot\mathbf{r}_{12}\}, \tag{42}$$

$$\langle\sigma_{22}^1\rangle_{\mathrm{ss}}^{[2]} + \langle\sigma_{22}^2\rangle_{\mathrm{ss}}^{[2]} = |g|^2|\overleftrightarrow{\boldsymbol{\Delta}}_{+1,+1}|^2\frac{R_2(s)}{P(s)}. \tag{43}$$

$R_1(s)$, $R_2(s)$, and $P(s)$ are polynomial expressions in the saturation parameter s,

$$R_1(s) = \frac{2}{9}(6912s + 3168s^2 + 264s^3 + 20s^4 + s^5), \tag{44a}$$

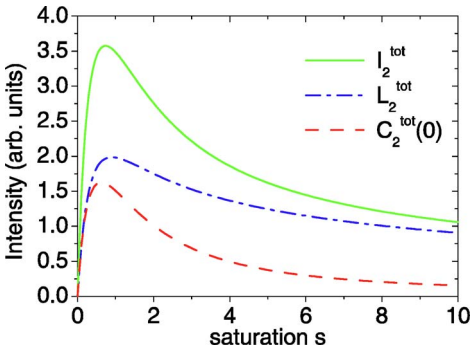

FIG. 3. (Color online) Saturation dependence of the total double-scattering contribution I_2^{tot} to the CBS signal in the $h\|h$ channel, decomposed in its ladder and interference parts L_2^{tot} and C_2^{tot}, according to Eqs. (46) and (47), at exact resonance $\delta=0$. At finite saturation s, the interference term C_2^{tot} drops below the ladder contribution L_2^{tot}, indicating a loss of coherence. At large $s\geq 1$, the total double-scattering intensity must decrease with s, since the scattering cross section of the emitting atom drops as s^{-1}.

$$R_2(s) = \frac{1}{3}(1152s + 528s^2 + 132s^3 + 7s^4), \tag{44b}$$

$$P(s) = (1+s)^2(12+s)(32+20s+s^2), \tag{44c}$$

and

$$\overleftrightarrow{\boldsymbol{\Delta}}_{q,q'} \equiv \hat{\mathbf{e}}_q\cdot\overleftrightarrow{\boldsymbol{\Delta}}\cdot\hat{\mathbf{e}}_{q'} \quad (q,q'=\pm 1,0). \tag{45}$$

The configuration average over Eqs. (43) and (42), defined in Eq. (38), leads to the final result

$$C_2^{\mathrm{tot}}(\theta) \simeq \frac{|\tilde{g}|^2 R_1(s)}{(4+s)P(s)}\left(\frac{2}{15} - \frac{(k\,\ell\,\theta)^2}{35}\right), \tag{46}$$

$$L_2^{\mathrm{tot}} = \frac{2|\tilde{g}|^2 R_2(s)}{15P(s)}, \tag{47}$$

with $\tilde{g}=g|_{r_{\alpha\beta}=\ell}$ [see Eq. (22)]. The scattering angle $\theta = 2\arcsin\{|\mathbf{k}+\mathbf{k}_L|/2k_L\}\ll 1$ with respect to the backscattering direction was assumed to be sufficiently small herein. A power series expansion of Eqs. (46) and (47) to second order in s reproduces the diagrammatically obtained result of [11]

$$C_2^{\mathrm{tot}} \propto s - \frac{5}{2}s^2, \quad L_2^{\mathrm{tot}} \propto s - \frac{9}{4}s^2, \tag{48}$$

for the total double-scattering intensity, at $\theta=0$.

The behavior of L_2^{tot} and $C_2^{\mathrm{tot}}(0)$ shows that the double-scattering intensity $I_2^{\mathrm{tot}}=L_2^{\mathrm{tot}}+C_2^{\mathrm{tot}}(0)$ behaves markedly different from that of an isolated atom. While the radiated intensity from an isolated atom,

$$I^{[0]} \propto \frac{s}{1+s}, \tag{49}$$

grows monotonically with s until it finally saturates [8], the double-scattering intensity exhibits a maximum at $s\simeq 0.7$ (see Fig. 3), followed by gradual decrease $\propto s^{-1}$ for large s. Also this is a simple consequence of the saturation behavior

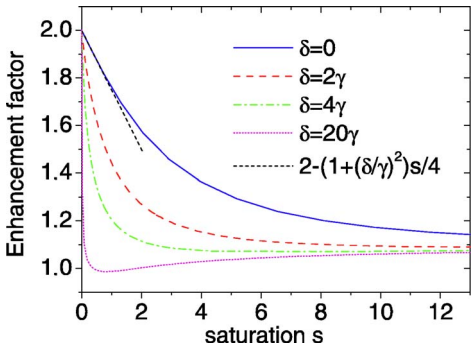

FIG. 4. (Color online) Numerical enhancement factor α in the helicity preserving channel $h\|h$, versus saturation s of the atomic transition, for different detunings δ from resonant driving. Larger detuning leads to a faster loss of the CBS contrast. At small s, one recovers the perturbative prediction [11] linear in s (straight dashed line). At large s, α saturates at a δ-dependent value $\alpha_{\delta_\infty} > 1$, due to the constructive self-interference of inelastically scattered photons. Remarkably, α also passes through a minimum at $s \simeq 0.5$, for very large detuning $\delta = 20\gamma$. This indicates *destructive* interference, and the physical cause of this observation remains to be identified.

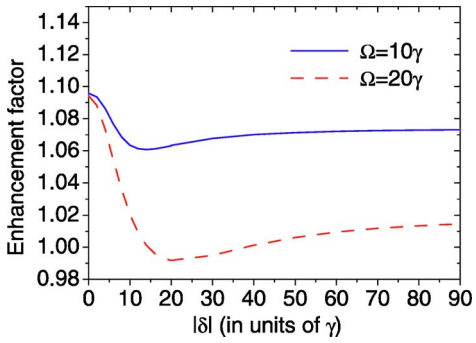

FIG. 5. (Color online) Numerical enhancement factor α (numerical solution) in the helicity preserving channel, versus the laser detuning δ, for two values of the driving Rabi frequency Ω. The decrease of α below unity for $\Omega = 20\gamma$, in the vicinity of $|\delta| = 20\gamma$, correlates with the minimum displayed by $\alpha(s)$ in the corresponding plot in Fig. 4, at $s \simeq 0.5$.

of an isolated atom described by (49): At high injected laser intensities, the atom that emits the final photon has a total scattering cross section that asymptotically decays like $I^{[0]}/I_L \propto s^{-1}$ [see Eqs. (1) and (11)] and is consequently less likely to scatter photons coming from the other atom.

The enhancement factor $\alpha(s)$, Eq. (41), deduced from Eqs. (46) and (47) reads

$$\alpha(s) = 1 + \frac{R_1(s)}{(4+s)R_2(s)}, \tag{50}$$

and $\alpha(0) = 2.0$ in the weak-field limit, as expected. The dependence of α on the saturation parameter is shown in Fig. 4. As above for the individual cross and ladder terms, we again obtain perfect agreement with the linear decay predicted by the scattering theoretical result $\alpha \simeq 2 - s/4$ [11], in the limit of small s. When s increases further, α monotonically drops to an asymptotic value $\lim_{s\to\infty}\alpha(s) = \alpha_\infty = 23/21$ which is strictly larger than unity, implying a nonvanishing residual CBS contrast in the limit of large injected intensities. As we shall see further down in Sec. IV A 3, this residual constructive interference effect is exclusively due to the (self-)interference of *inelastically* scattered photons.

2. Finite detuning

It is in general no more possible to obtain explicit expressions for the Green's matrix $\mathbf{G}_0$ (tantamount of inverting $\mathbf{A}$), in the case of nonvanishing detuning $\delta \neq 0$. However, this can always be done numerically, and Fig. 4 compares the enhancement factor at resonance to the one for three different nonvanishing values of δ. In qualitative agreement with the experiment [6], α decays faster for larger detuning, as s is increased from zero. But not only does the enhancement factor exhibit a steeper (initial) decrease with δ: it also reveals *destructive* interference ($\alpha < 1$) for large detuning $\delta = 20\gamma$, at $s \simeq 0.5$. This corresponds to a large Rabi frequency $\Omega \simeq 20\gamma$.

To gain some insight on whether such destructive interference is generic for large Rabi frequencies and large detunings, we monitor enhancement factor versus detuning, for two fixed, large values of the Rabi frequency, as displayed in Fig. 5. For a given value of Ω, the enhancement factor decreases as a function of $|\delta|$, from its maximum at $\delta = 0$ to its Ω-dependent minimum value at $|\delta| \simeq \Omega$. For very large detunings, α_δ saturates at a level $1 < \lim_{|\delta|\to\infty}\alpha_\delta = \alpha_{\delta_\infty} < \alpha_\infty$, indicating (i) constructive (self-)interference of far-detuned photons and (ii) similar behavior of the ladder and crossed terms, asymptotically in $|\delta|$. The asymptotic value α_{δ_∞} is the lower the larger Ω. Furthermore, as a direct counterpart of the destructive interference observed in Fig. 4, α drops below unity for $\Omega = 20\gamma$, in a finite range of $|\delta|$.

Note that a similar effect was predicted in [22], for linear double scattering from atoms with Zeeman-shifted hyperfine ground levels. In our case, the onset of destructive interference at $\delta \simeq 15\gamma$ and $s_0 \simeq \Omega^2/2\gamma^2 = 200$ occurs approximately at saturation $s \simeq 0.9$. A physical interpretation of this interference-induced *antienhancement* of CBS, which we tentatively attribute to an ac Stark shift of the laser-driven atomic sublevels, will require a closer inspection of the total stationary intensity and is referred to a separate contribution.

3. Elastic component at finite detuning

To see that the residual contrast observed in Fig. 4 for large saturation parameters stems from inelastically scattered photons, we now derive expressions for the elastic ladder and crossed contributions to the double-scattering CBS signal. To do so, we extract the elastic contribution I_2^{el} to the total double-scattering intensity from an expansion of Eq. (37) to second order in $|g|$, as prescribed by Eqs. (34) and (35):

$$I_2^{\mathrm{el}} = |\langle\sigma_{21}^1\rangle_{\mathrm{ss}}^{[1]}|^2 + |\langle\sigma_{21}^2\rangle_{\mathrm{ss}}^{[1]}|^2 + 2\,\mathrm{Re}(\langle\sigma_{21}^1\rangle_{\mathrm{ss}}^{[1]}\langle\sigma_{12}^2\rangle_{\mathrm{ss}}^{[1]} e^{i\mathbf{k}\cdot\mathbf{r}_{12}}). \tag{51}$$

With the evolution equations

$$\langle\dot{\sigma_{12}^\alpha}\rangle = (-\gamma + i\delta)\langle\sigma_{12}^\alpha\rangle - \frac{i}{2}\Omega_\alpha\langle\sigma_{42}^\alpha\rangle + \sum_{i,j} T_{ij}\langle Q_i^\alpha Q_j^\beta\rangle, \tag{52a}$$

$$\dot{\langle\sigma_{42}^{\alpha}\rangle} = -2\gamma\langle\sigma_{42}^{\alpha}\rangle - \frac{i}{2}\Omega_{\alpha}^{*}\langle\sigma_{12}^{\alpha}\rangle + \sum_{i,j} T_{ij}\langle Q_i^{\alpha} Q_j^{\beta}\rangle, \quad (52b)$$

which can be derived from Eqs. (19)–(21), an analytic expression for the steady-state mean value $\langle\sigma_{12}^{\alpha}\rangle_{ss}^{[1]}$ and thus for I_2^{el} is obtained by the following argument (note that this remains valid also for finite detuning δ): As long as we content ourselves with a lowest-order treatment of multiple-scattering effects, only factorized zeroth-order correlation functions $\langle Q_i^{\alpha}\rangle_{ss}^{[0]}\langle Q_j^{\beta}\rangle_{ss}^{[0]}$ for independent atoms $\alpha \neq \beta$ contribute to the sums on the right-hand side of Eqs. (52a) and (52b), since the coefficients T_{ij} are of order $|g|$, expressing the dipole-dipole interaction between distinct atoms. Such products vanish except if their factors involve only the driven levels $|1\rangle_{\alpha}$ or $|4\rangle_{\beta}$. Consequently, the summations in Eqs. (52a) and (52b), which extend over different subsets of the two-atom correlation functions, can be condensed according to

$$\sum_{i,j} T_{ij}\langle Q_i^{\alpha}\rangle_{ss}^{[0]}\langle Q_j^{\beta}\rangle_{ss}^{[0]} \to \gamma g^{*}\overleftrightarrow{\Delta}_{+1,+1}\langle\sigma_{14}^{\beta}\rangle_{ss}^{[0]}\langle\sigma_{11}^{\alpha}\rangle_{ss}^{[0]}, \quad (53)$$

$$\sum_{i,j} T_{ij}\langle Q_i^{\alpha}\rangle_{ss}^{[0]}\langle Q_j^{\beta}\rangle_{ss}^{[0]} \to \gamma g^{*}\overleftrightarrow{\Delta}_{+1,+1}\langle\sigma_{14}^{\beta}\rangle_{ss}^{[0]}\langle\sigma_{41}^{\alpha}\rangle_{ss}^{[0]}, \quad (54)$$

respectively. Substitution thereof into Eqs. (52a) and (52b) [with the left-hand side of Eqs. (52a) and (52b) equal to zero, and $\langle\sigma_{14}^{\alpha}\rangle = \langle\sigma_{41}^{\alpha}\rangle^{*}$], together with the known solutions of the optical Bloch equations for a single two-level atom [8],

$$\langle\sigma_{14}^{\alpha}\rangle_{ss}^{[0]} = \frac{i(\gamma + i\delta)}{\Omega_{\alpha}^{*}}\frac{s}{1+s}, \quad \langle\sigma_{11}^{\alpha}\rangle_{ss}^{[0]} = \frac{2+s}{2(1+s)}, \quad (55)$$

leads to

$$\langle\sigma_{12}^{\alpha}\rangle_{ss}^{[1]} = \frac{i\gamma g^{*}\overleftrightarrow{\Delta}_{+1,+1}\Omega_{\beta}}{2(\gamma - i\delta)^2(1+s)^2}. \quad (56)$$

If we now rewrite Eq. (51) as

$$I_2^{el} = |T_{dir} + T_{rev}|^2, \quad (57)$$

with $T_{dir} \equiv \langle\sigma_{12}^{1}\rangle_{ss}^{[1]} e^{-i\mathbf{k}\cdot\mathbf{r}_1}$ and $T_{rev} \equiv \langle\sigma_{12}^{2}\rangle_{ss}^{[1]} e^{-i\mathbf{k}\cdot\mathbf{r}_2}$, the elastic component of the double-scattering intensity appears, with Eq. (11), as the square modulus of a sum of the "direct" and "reversed" scattering amplitudes

$$T_{dir} = \frac{i\gamma g^{*}\overleftrightarrow{\Delta}_{+1,+1}\Omega}{2(\gamma - i\delta)^2(1+s)^2} e^{i\mathbf{k}_L\cdot\mathbf{r}_2 - i\mathbf{k}\cdot\mathbf{r}_1}, \quad (58)$$

$$T_{rev} = \frac{i\gamma g^{*}\overleftrightarrow{\Delta}_{+1,+1}\Omega}{2(\gamma - i\delta)^2(1+s)^2} e^{i\mathbf{k}_L\cdot\mathbf{r}_1 - i\mathbf{k}\cdot\mathbf{r}_2}. \quad (59)$$

Direct and reverse amplitudes are symmetric under the interchange $\mathbf{k} \leftrightarrow -\mathbf{k}_L$ and thus satisfy the condition of reciprocity [17]. Consequently, the elastically scattered photons remain strictly coherent, for any s, and show perfect CBS contrast with $\alpha(s)=2$, as immediately spelled out by the explicit expression for the elastic ladder and crossed terms, at arbitrary detuning and Rabi frequency:

$$L_2^{el} = C_2^{el}(0) = \frac{2|\tilde{g}|^2}{15}\frac{1}{1+(\delta/\gamma)^2}\frac{s}{(1+s)^4}. \quad (60)$$

While perfectly coherent even for large s, the elastic contribution to the total double-scattering intensity decreases as s^{-3}, by virtue of Eq. (60), after passing through a maximum at $s=1/3$. In contrast, the total signal fades away like s^{-1}, according to Eqs. (46) and (47). Consequently, in the large-s limit, the CBS signal is completely dominated by the inelastic scattering component and the residual CBS contrast α_{∞} observed in Sec. IV A 1 above is due to the selfinterference of inelastically scattered photons, which are incoherent with respect to the injected laser radiation. The visibility of this residual interference signal is limited by the amount of which-way information communicated to the environment, during the multiple-scattering process [23].

Finally, let us note that Eq. (60) allows for a transparent interpretation, since it can be factorized into (i) the elastic intensity

$$I^{el[0]} \propto \frac{s}{(1+s)^2} \quad (61)$$

scattered by the first strongly driven atom, (ii) the total scattering cross section

$$\sigma^{tot} \propto \frac{1}{(1+(\delta/\gamma)^2)(1+s)} \quad (62)$$

of the second atom, and (iii) the relative weight $I^{el[0]}/I^{tot[0]} = \sigma^{el}/\sigma^{tot}$ equal to

$$\frac{\gamma^2 + \delta^2}{\gamma^2 + \Omega^2/2 + \delta^2} = \frac{1}{1+s} \quad (63)$$

of elastic processes [8].

B. lin ⊥ lin channel

Up to a constant factor of 1/2, the results for the lin ⊥ lin channel turn out to be the same as for the $h\|h$ channel, at exact backscattering. For a given value of s, the ladder and crossed terms are 2 times smaller than in the $h\|h$ channel. Since, however, Eq. (16) for the intensity in the lin ⊥ lin channel is manifestly different from Eq. (15), the $h\|h$ result, a short discussion of this observation is in order.

In both cases, the CBS intensity is observed in the polarization channel orthogonal to the excitation channel. In the $h\|h$ channel, the orthogonal channel is defined by one dipole transition $|2\rangle \to |1\rangle$. In the lin ⊥ lin channel, the orthogonal channel is defined by two atomic transitions $|2\rangle \to |1\rangle$ and $|4\rangle \to |1\rangle$. Yet, by introducing a superposition state $|e\rangle \equiv |2\rangle + |4\rangle$, we can rewrite expression (16) in a way which is formally equivalent to Eq. (15). However, the geometric weight of the resulting ladder and crossed intensities is given by $(\overleftrightarrow{\Delta}_{0,-1} + \overleftrightarrow{\Delta}_{0,+1})(\overleftrightarrow{\Delta}_{+1,0} + \overleftrightarrow{\Delta}_{-1,0})/2$. Only two of these four terms, $\overleftrightarrow{\Delta}_{0,-1}\overleftrightarrow{\Delta}_{-1,0}/2$ and $\overleftrightarrow{\Delta}_{0,+1}\overleftrightarrow{\Delta}_{+1,0}/2$, survive the configuration average, which leads to results that are two times smaller than in the $h\|h$ channel.

C. $h \perp h$ channel

We shall now consider detected photons which have the same polarization as the incident ones. Hence, as already briefly discussed in Sec. II F, single-scattering as well as double-scattering events will contribute to the detected signal, with the latter only a small correction to the former. Correspondingly, an experimental detection of the double-scattering contribution alone is excluded. Nonetheless, it is instructive to consider this scenario in the regime of a nonlinear atomic response to the injected radiation because it allows us to identify the role of recurrent scattering where one photon rescatters from the same atom, after visiting the other (this process is second order in the coupling constant $|g|$).

1. Total intensity

To obtain explicit expressions for the total scattered intensity, we proceed stepwise and first expand the single-atom contribution to the intensity, in Eq. (17), to second order in g. We obtain

$$\sum_{\alpha=1}^{2} \langle \sigma_{44}^{\alpha} \rangle_{\mathrm{ss}}^{[2]} = |g|^2 [F_1(s) |\overleftrightarrow{\mathbf{\Delta}}_{+1,-1}|^2 + F_2(s)(|\overleftrightarrow{\mathbf{\Delta}}_{+1,0}|^2 + |\overleftrightarrow{\mathbf{\Delta}}_{+1,+1}|^2)] + \text{terms} \propto \mathrm{Re}[g^2], |g|^2 \cos\{2\mathbf{k}_L \cdot \mathbf{r}_{12}\}, \tag{64}$$

where

$$F_1(s) = \frac{36s + 3s^2 - 27s^3 - 19s^4 - s^5}{12(1+s)^5(3+s)}, \tag{65}$$

$$F_2(s) = -\frac{4s^2(288 + 132s + 23s^2 + s^3)}{3(1+s)P(s)}, \tag{66}$$

with $P(s)$ from Eq. (44). The terms in the last line of Eq. (64) oscillate rapidly on the typical scale ℓ of the interatomic separation [recall Eq. (22) and $k_0 r_{\alpha\beta} \gg 1$; this is, also, the dependence of g on r_{12} is to be taken into account here] and average out under the integral over r_{12} in Eq. (38). Thus, they will be dropped hereafter, whereas terms $\propto |g|^2 = 9/4k_0^2 r_{12}^2$ vary smoothly with r_{12} and will be kept.

An analogous expansion of the interference terms in Eq. (17) yields the expression

$$2\,\mathrm{Re}\{\langle \sigma_{41}^1 \sigma_{14}^2 \rangle_{\mathrm{ss}}^{[2]} e^{i\mathbf{k}\cdot\mathbf{r}_{12}}\} = |g|^2 F_3(s) |\overleftrightarrow{\mathbf{\Delta}}_{+1,-1}|^2 \times \cos\{(\mathbf{k} + \mathbf{k}_L) \cdot \mathbf{r}_{12}\} + \text{terms} \propto \mathrm{Re}[g^2], |g|^2 \cos\{(\mathbf{k} - \mathbf{k}_L) \cdot \mathbf{r}_{12}\}, |g|^2 \cos\{(3\mathbf{k}_L - \mathbf{k}) \cdot \mathbf{r}_{12}\}, \tag{67}$$

where

$$F_3(s) = \frac{324s + 540s^2 + 450s^3 + 219s^4 + 85s^5 + 29s^6 + s^7}{36(1+s)^6(3+s)^2}. \tag{68}$$

The three last lines of Eq. (67) are irrelevant for our subsequent treatment, for exactly the same reason as the corresponding terms in Eq. (64).

We now have a closer look at the geometric factors in these equations, which allow the identification of the underlying elementary scattering processes. The geometric weight of the contribution proportional to $F_2(s)$ in Eq. (64) is given by $|\overleftrightarrow{\mathbf{\Delta}}_{+1,0}|^2 + |\overleftrightarrow{\mathbf{\Delta}}_{+1,+1}|^2$. It describes the coupling of a photon from the $|4\rangle_\alpha \to |1\rangle_\alpha$ transition either to the $|3\rangle_\beta \to |1\rangle_\beta$ or to the $|2\rangle_\beta \to |1\rangle_\beta$ transition, respectively, then back to the $|4\rangle_\alpha \to |1\rangle_\alpha$ transition, and only then to a detector. This is recurrent scattering. (Note that nonrecurrent transitions—e.g., from $|4\rangle_\alpha \to |1\rangle_\alpha$ to $|3\rangle_\beta \to |1\rangle_\beta$ or to $|2\rangle_\beta \to |1\rangle_\beta$—cannot give rise to a detected photon in the $h \perp h$ channel.)

More precisely, the single-scattering contribution with weight $F_2(s)$ originates from interference between single scattering from independent atoms and (recurrent) triple scattering, in which a photon is subsequently scattered by atom α, then by atom β, and by atom α again [recall our discussion in Sec. II F, and also see Eqs. (72) and (73) in our subsequent discussion of the elastic contribution to the $h \perp h$ channel]. Since the rate of single and recurrent scattering is equally limited by the number of photons incident on the atom, $\propto s$, it follows that $F_2(s) \propto s^2$ for $s \to 0$. This is consistent with a basic postulate of multiple-scattering theory [19], according to which recurrent scattering is irrelevant in the linear regime of weak saturation. It is also clear why there is no recurrent scattering in $h \| h$ and $\mathrm{lin} \perp \mathrm{lin}$ channels: Indeed, single scattering is essential for recurrent scattering to show up at order $|g|^2$, but is filtered out in the orthogonal polarization channels.

Now consider those terms in Eqs. (64) and (67) with angular part $|\overleftrightarrow{\mathbf{\Delta}}_{+1,-1}|^2$. Along with the processes in which atoms exchange photons, these equally much represent the two recurrent-scattering sequences $|4\rangle_\alpha \to |4\rangle_\beta \to |4\rangle_\alpha$. The weight of these contributions is not the same as for $|4\rangle_\alpha \to |3\rangle_\beta \to |4\rangle_\alpha$ and $|4\rangle_\alpha \to |2\rangle_\beta \to |4\rangle_\alpha$ transitions, since the presence of the driving field in the $|1\rangle \leftrightarrow |4\rangle$ transition definitely destroys the symmetry of the excited state sublevels.

As regards the sign of the various scattering contributions in Eqs. (64) and (67), note that the weight of the interference part given by Eq. (68) is positive for all s, while $F_1(s)$ and $F_2(s)$, Eqs. (65) and (66) are nonpositive, the function $F_2(s)$ being strictly negative for $s \neq 0$. Hence, recurrent scattering is a small negative correction to the overall positive single-atom contribution to the total scattering signal.

The total crossed and ladder contributions to the double-scattering intensity are once again obtained after a final configuration average of Eqs. (64) and (67):

$$L_2^{\mathrm{tot}} = \frac{1}{15} |\tilde{g}|^2 [7F_1(s) + 3F_2(s)], \tag{69}$$

$$C_2^{\mathrm{tot}}(0) = \frac{7}{15} |\tilde{g}|^2 F_3(s). \tag{70}$$

The result is plotted in Fig. 6, where L_2^{tot} turns negative in a finite interval of s. In the limit of large s, the ladder term approaches zero from below, as $1/s$, whereas the crossed terms decreases towards zero, with the same rate $1/s$. Note that the negativity of the ladder term is compensated for by the single-scattering contribution L_1 which cannot be sepa-

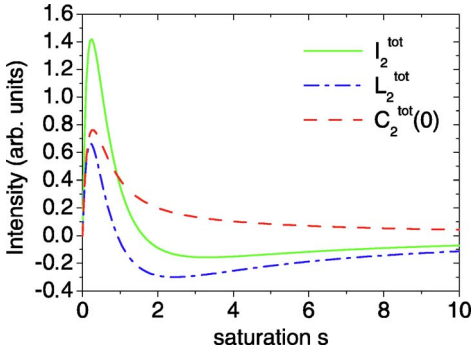

FIG. 6. (Color online) Total crossed [Eqs. (70)] and ladder [Eq. (69)] terms, together with the double-scattering intensity $I_2^{\mathrm{tot}}=L_2^{\mathrm{tot}}+C_2^{\mathrm{tot}}(0)$, in the $h\perp h$ channel, as functions of the saturation s, at exact resonance $\delta=0$.

rated from the double-scattering contribution, in the $h\perp h$ channel. Furthermore, the single-scattering contribution does not decrease with growing s but rather saturates, so that for very large saturation parameters we can simply ignore the double-scattering contribution. For all s, the CBS enhancement factor reads, after inclusion of L_1,

$$\alpha = 1 + \frac{C_2^{\mathrm{tot}}(0)}{L_1 + L_2^{\mathrm{tot}}}. \tag{71}$$

In a real medium, the relative weight of single and double scattering depends on the optical thickness. However, our simple model cannot correctly account for this effect; hence, we cannot assess here whether the negativity of the double-scattering ladder term has observable consequences in laboratory experiments.

2. Elastic component

Let us finally extract the elastic component of the CBS intensity in the $h\perp h$ channel. According to Eqs. (17) and (36), with Eq. (38), the elastic ladder and crossed terms are given by

$$L_2^{\mathrm{el}} = 2\langle|\langle\sigma_{41}^1\rangle_{\mathrm{ss}}^{[1]}|^2 + \langle\sigma_{41}^1\rangle_{\mathrm{ss}}^{[0]}\langle\sigma_{14}^1\rangle_{\mathrm{ss}}^{[2]} + \langle\sigma_{41}^1\rangle_{\mathrm{ss}}^{[2]}\langle\sigma_{14}^1\rangle_{\mathrm{ss}}^{[0]}\rangle_{\mathrm{conf}}, \tag{72}$$

$$C_2^{\mathrm{el}}(\theta) = 2\,\mathrm{Re}\langle e^{i\mathbf{k}\cdot\mathbf{r}_{12}}(\langle\sigma_{41}^1\rangle_{\mathrm{ss}}^{[1]}\langle\sigma_{14}^2\rangle_{\mathrm{ss}}^{[1]} + \langle\sigma_{41}^1\rangle_{\mathrm{ss}}^{[0]}\langle\sigma_{14}^2\rangle_{\mathrm{ss}}^{[2]} + \langle\sigma_{41}^1\rangle_{\mathrm{ss}}^{[2]}\langle\sigma_{14}^2\rangle_{\mathrm{ss}}^{[0]})\rangle_{\mathrm{conf}}. \tag{73}$$

Due to the factorization (36) of the classically radiating dipoles, symmetric and asymmetric scattering contributions are directly born out: Products of first-order (labeled by [1]) contributions in g represent double scattering of photons subsequently at atoms 1 and 2, in direct and reversed order, whereas products of zero and second order ([0] and [2], respectively) express indistinguishable single-scattering and recurrent-scattering amplitudes upon either one of the atoms. Explicitly, the above expressions have the following geometric weights:

$$L_2^{\mathrm{el}} = \langle|g|^2|\overleftrightarrow{\Delta}_{+1,-1}|^2\rangle_{\mathrm{conf}}\left[\frac{s+s^3}{(1+s)^6} + F_4(s)\right] + \langle|g|^2(|\overleftrightarrow{\Delta}_{+1,0}|^2 + |\overleftrightarrow{\Delta}_{+1,+1}|^2)\rangle_{\mathrm{conf}} \times \frac{2F_2(s)}{1+s}, \tag{74}$$

$$C_2^{\mathrm{el}}(\theta) = \langle|g|^2|\overleftrightarrow{\Delta}_{+1,-1}|^2\cos\{(\mathbf{k}+\mathbf{k}_L)\cdot\mathbf{r}_{12}\}\rangle_{\mathrm{conf}} \times\left[\frac{s}{(1+s)^6} + F_5(s)\right], \tag{75}$$

where all terms which vanish under the configuration average have already been dropped [see also the discussion of Eqs. (64) and (67) above] and

$$F_4(s) = \frac{-36s^2 - 39s^3 - 14s^4 + s^5}{3(1+s)^6(3+s)}, \tag{76}$$

$$F_5(s) = \frac{-72s^2 - 51s^3 - s^4 + 3s^5 + s^6}{12(1+s)^6(3+s)}. \tag{77}$$

Upon evaluation of the configuration average, we obtain the final result

$$L_2^{\mathrm{el}} = |\tilde{g}|^2\frac{7}{15}\left[\frac{s+s^3}{(1+s)^6} + F_4(s) + \frac{6}{7}\frac{F_2(s)}{1+s}\right], \tag{78}$$

$$C_2^{\mathrm{el}}(0) = |\tilde{g}|^2\frac{7}{15}\left[\frac{s}{(1+s)^6} + F_5(s)\right]. \tag{79}$$

Expressions (78) and (79) imply that, in the small-s limit, the elastic ladder and crossed terms coincide, as for orthogonal polarization channels [see Eq. (60)]. However, this equipartition does *not* prevail here beyond the linear regime, due to reciprocity-violating processes [11], which lead to a deviation of L_2^{el} from $C_2^{\mathrm{el}}(0)$, already at quadratic order in s. The violation of reciprocity was originally demonstrated in [11] for scalar atoms, and it will be demonstrated below in Sec. IV E that the scalar results immediately follow from our present results for parallel excitation and detection polarization channels, when ignoring those electronic sublevels that mediate recurrent scattering. However, beyond those reciprocity-violating processes already implicit in the scalar treatment, other processes specifically due to the vector character of the injected radiation field lead to additional deviations [expressed by the term $\propto F_2(s)$ in Eq. (78)].

Furthermore, note that the elastic ladder and crossed intensities in the $h\perp h$ channel asymptotically behave like $\propto 1/s^2$ and $\propto 1/s$, respectively. Also the total double-scattering intensity in this channel is characterized by an asymptotic decrease $\propto 1/s$ (see Sec. IV C 1). Consequently, unlike the $h\|h$ channel, where double scattering becomes purely inelastic for large s, here both elastic *and* inelastic photons are present for large s.

D. lin∥lin channel

The results for the lin∥lin channel are the same as for the $h\perp h$ channel, modulo the following substitution of the geometric weights:

$$|\vec{\Delta}_{+1,-1}|^2 \to |\vec{\Delta}_{0,0}|^2, \quad |\vec{\Delta}_{+1,+1}|^2 \to |\vec{\Delta}_{-1,0}|^2. \tag{80}$$

This entails slightly different final expressions for the ladder and crossed terms. For the total intensities, we obtain

$$L_2^{\mathrm{tot}} = \frac{1}{15}|\tilde{g}|^2[8F_1(s) + 2F_2(s)], \tag{81}$$

$$C_2^{\mathrm{tot}}(0) = \frac{8}{15}|\tilde{g}|^2 F_3(s), \tag{82}$$

and the elastic result reads

$$L_2^{\mathrm{el}} = |\tilde{g}|^2 \frac{8}{15}\left[\frac{s+s^3}{(1+s)^6} + \frac{F_2(s)}{2(1+s)} + F_4(s)\right], \tag{83}$$

$$C_2^{\mathrm{el}}(0) = |\tilde{g}|^2 \frac{8}{15}\left[\frac{s}{(1+s)^6} + F_5(s)\right]. \tag{84}$$

Eqs. (81)–(84) differ from Eqs. (69), (70), (78), and (79) only through numerical coefficients. Therefore, all our above conclusions for the elastic and inelastic components of double scattering in the $h \perp h$ channel also apply for the present lin$\|$lin case.

E. Scattering of scalar photons on a two-level atom

To conclude, let us briefly consider the model scenario of scalar photons scattering on a two-level atom—a wide spread setting in typical quantum-optical model calculations, which neglects the important role of the polarization degree of freedom in the presently discussed quantum transport problem. The scalar case is easily deduced from the above results for the $h \perp h$ or lin$\|$lin channels, by simply setting equal to zero those contributions with the geometric weight $|\vec{\Delta}_{+1,0}|^2 + |\vec{\Delta}_{+1,+1}|^2$—since a two-level atom does not offer the required atomic transitions.

The total ladder and crossed terms then read, by virtue of Eqs. (64), (67), (69), and (70),

$$L_2^{\mathrm{tot}} = \frac{7}{15}|\tilde{g}|^2 F_1(s), \tag{85}$$

$$C_2^{\mathrm{tot}}(0) = \frac{7}{15}|\tilde{g}|^2 F_3(s), \tag{86}$$

with the quadratic expansion

$$L_2^{\mathrm{tot}} \propto s - \frac{21}{4}s^2, \quad C_2^{\mathrm{tot}}(0) \propto s - 5s^2, \tag{87}$$

in precise agreement with the result of [11].

Correspondingly, the elastic contributions, Eqs. (78) and (79), reduce to

$$L_2^{\mathrm{el}} = |\tilde{g}|^2 \frac{7}{15}\left[\frac{s+s^3}{(1+s)^6} + F_4(s)\right], \tag{88}$$

$$C_2^{\mathrm{el}}(0) = |\tilde{g}|^2 \frac{7}{15}\left[\frac{s}{(1+s)^6} + F_5(s)\right], \tag{89}$$

which once again reproduces the second-order expressions

$$L_2^{\mathrm{el}} \propto s - 10s^2, \quad C_2^{\mathrm{el}}(0) \propto s - 8s^2 \tag{90}$$

of [11].

Thus, the scalar model correctly predicts the maximum enhancement factor $\alpha = 2$, in the elastic scattering limit $s \to 0$. Furthermore, it correctly describes those CBS contributions in the parallel excitation and detection channels which originate from the laser-driven transitions, for arbitrary s. However, the scalar model in general leads to incorrect results, since it ignores contributions from those sublevels of the degenerate excited state which are not driven by the laser, yet mediate recurrent scattering, as we have seen in Sec. IV C 1.

V. SUMMARY

In summary, we have given a detailed account of the master-equation treatment of the coherent backscattering of light from a disordered sample of cold atoms with a nondegenerate electronic ground state. This approach extracts all physical observables from the steady-state expectation values of atomic-dipole operators. Furthermore, our treatment incorporates the effect of interatomic dipole-dipole interactions for *distant* atoms.

In particular, the formalism allows us to treat arbitrary pump intensities which possibly saturate the relevant atomic transitions, thus leading to inelastic scattering events (when more than one photon is incident on the scattering atom—on the spectral level, this entails the emergence of the famous Mollow triplet, in a single atom's fluorescence). The price to pay is a rapidly increasing dimension of the Hilbert space spanned by the many atoms' degrees of freedom. This limited our present treatment to two atomic scatterers, which is the minimum number of constituents to observe the CBS effect. Nonetheless, this approach allowed us to show that a small residual CBS signal survives even in the limit of purely inelastic scattering, due to the self-interference of inelastically scattered photons.

Furthermore, we have seen that recurrent scattering leads to a reduction of the total double-scattering signal, due to a destructive interference between single- and triple-scattering events upon the same atomic scatterer.

Another advantage of the master-equation treatment presented here, so far unexplored, is the immediate availability of the CBS *spectrum* through a Fourier transform of suitable atomic-dipole correlation functions, as well as of the associated photocount statistics. Whether CBS has an unambiguous signature in the spectrum and/or in the photocurrent remains hitherto an open question, but is becoming in reach for state-of-the-art experiments.

ACKNOWLEDGMENTS

It is a pleasure to acknowledge entertaining and enlightening discussions with Dominique Delande, Benoît Grémaud, Christian Miniatura, Thomas Wellens, Eugene Petrov, and Carlos Viviescas.

[1] *Mesoscopic Quantum Physics*, edited by E. Akkermans, G. Montambaux, J.-L. Pichard, and J. Zinn-Justin (Elsevier, Amsterdam, 1994).
[2] P. Sheng, *Introduction to Wave Scattering, Localization and Mesoscopic Phenomena* (Academic Press, San Diego, 1995).
[3] Y. Kuga and A. Ishimaru, J. Opt. Soc. Am. A **1**, 831 (1984); M. P. Van Albada and A. Lagendijk, Phys. Rev. Lett. **55**, 2692 (1985); P. E. Wolf and G. Maret, *ibid.* **55**, 2696 (1985).
[4] G. Labeyrie, F. de Tomasi, J.-C. Bernard, C. A. Müller, C. Miniatura, and R. Kaiser, Phys. Rev. Lett. **83**, 5266 (1999).
[5] P. Kulatunga, C. I. Sukenik, S. Balik, M. D. Havey, D. V. Kupriyanov, and I. M. Sokolov, Phys. Rev. A **68**, 033816 (2003).
[6] T. Chanelière, D. Wilkowski, Y. Bidel, R. Kaiser, and C. Miniatura, Phys. Rev. E **70**, 036602 (2004).
[7] C. A. Müller and C. Miniatura, J. Phys. A **35**, 10163 (2002).
[8] C. Cohen-Tannoudji, J. Dupont-Roc, and G. Grynberg, *Atom-Photon Interactions* (Wiley, New York, 1992).
[9] H. Cao, Y. Ling, J. Y. Xu, C. Q. Cao, and Prem Kumar, Phys. Rev. Lett. **86**, 4524 (2001).
[10] G. Labeyrie, D. Delande, C. A. Müller, C. Miniatura, and R. Kaiser, Europhys. Lett. **61**, 327 (2003).
[11] T. Wellens, B. Grémaud, D. Delande, and C. Miniatura, Phys. Rev. A **70**, 023817 (2004).
[12] B. Grémaud, T. Wellens, D. Delande, and C. Miniatura, e-print quant-ph/0506010.
[13] V. Shatokhin, C. A. Müller, and A. Buchleitner, Phys. Rev. Lett. **94**, 043603 (2005).
[14] H. J. Carmichael, *An Open System Approach to Quantum Optics* (Springer, New York, 1993).
[15] R. H. Lehmberg, Phys. Rev. A **2**, 883 (1970); D. F. V. James, *ibid.* **47**, 1336 (1993); J. Guo and J. Cooper, *ibid.* **51**, 3128 (1995).
[16] In the above, $\hat{n}\hat{n}$ and $\hat{\mathbf{e}}_i\hat{\mathbf{e}}_j$ have to be read as dyadic products.
[17] T. Jonckheere, C. A. Müller, R. Kaiser, C. Miniatura, and D. Delande, Phys. Rev. Lett. **85**, 4269 (2000).
[18] Y. Bidel, B. Klappauf, J. C. Bernard, D. Delande, G. Labeyrie, C. Miniatura, D. Wilkowski, and R. Kaiser, Phys. Rev. Lett. **88**, 203902 (2002).
[19] A. Lagendijk and B. A. van Tiggelen, Phys. Rep. **270**, 143 (1996).
[20] D. S. Wiersma, M. P. van Albada, B. A. van Tiggelen, and A. Lagendijk, Phys. Rev. Lett. **74**, 4193 (1995).
[21] C. A. Müller, T. Jonckheere, C. Miniatura, and D. Delande, Phys. Rev. A **64**, 053804 (2001).
[22] D. V. Kupriyanov, I. M. Sokolov, and M. D. Havey, Opt. Commun. **243**, 165 (2004).
[23] B.-G. Englert, Phys. Rev. Lett. **77**, 2154 (1996).